A&A 367, 33–45 (2001)
DOI: 10.1051/0004-6361:20000417
© ESO 2001

Astronomy & Astrophysics

The 1 to 2.5 μ broad band emission of Blue Compact Dwarf Galaxies⋆

V. Doublier[1,3], A. Caulet[2], and G. Comte[3]

[1] European Southern Observatory, Alonso de Cordova 3107, Casilla 19, Vitacura, Santiago, Chile
[2] Calypso Observatory, Kitt Peak Observatory 950 North Cherry avenue, Tuscon, AR 85719, USA
[3] Observatoire de Marseille and Institut Gassendi, (CNRS), 2 place Le Verrier, 13248 Marseille Cedex 04, France

Received 8 November 1999 / Accepted 29 November 2000

Abstract. We present J, H and K surface photometry of 12 Blue Compact Dwarf Galaxies (BCDGs) selected from the southern sample (Doublier et al. 1999). A systematic excess of light in the K band with respect to the other bands in the visible and the near infrared is observed, indicating, since nebular emission is negligible, that a stellar population of red giants dominates the global flux from the galaxy. Moreover, comparisons of the metallicity-color relations of BCDGs and globular clusters show very little differences, indicating that BCDGs are most probably old, in the cosmological sense, systems. Local colors of the star forming regions show that these regions are indeed very young and possibly coeval across the galaxy when several starburst locations exist. At least 4 BCDGs (UM 465A and B, Haro 14 and Tololo 0610-378) show evidence of the presence of young red supergiant stars. The light distributions in the J, H and K bands are generally consistent with those in the optical, the differences are discussed. We confirm that our optical photometric classification remains valid in the near infrared. Thus, the global light distribution in the galaxy is an intrinsic property of the host galaxy independent of the presence of the starburst.

Key words. galaxies: compact – dwarf – fundamental parameters – stellar content

1. Introduction

Blue Compact Dwarf Galaxies (hereafter BCDGs) have attracted attention because they present extreme properties, such as low metallicities, high star formation rates, and an apparent low dust content (Thuan et al. 1999). Their study helps understanding star formation processes in atypical environments. The discovery of I ZW 18 and SBS 0335-052 believed to be genuine young systems massively forming stars for the first time, has stimulated the search for other cases (I ZW 18: Kunth & Sagent 1986; SBS 0335-052: Thuan et al. 1997). The ultimate goal of this search is the characterization of zero-redshift analogs to high z primeval galaxies. However, early studies in the near infrared conducted by Thuan (1983) and Hunter & Gallagher (1985), showed that an evolved population seemed to be present in the BCDGs they observed. The post-starburst phase of BCDGs is poorly known, but they are believed to be the intermediate phase between the dwarf irregulars (dIs) and the dwarf spheroidals (dEs) (Papaderos et al. 1996; Telles 1996). However, recent observations that a large fraction of BCDGs have dominant $r^{1/4}$ brightness distribution profiles (Doublier et al. 1997, 1999, hereafter Papers I and II), whereas all known dIs and almost all observed dEs have dominant exponential light profiles. The $r^{1/4}$ profile suggests that the system is, at least partly, dynamically relaxed, and it is most unlikely that an $r^{1/4}$ BCDG will evolve into an exponential dwarf spheroidal galaxy. Moreover, the observed sub-structures in BCDGs are associated with the starburst itself, and the evolved stages of these structures, i.e. once the star formation has faded away, are yet to be determined. In that respect, Ferguson & Binggeli (1994) made a distinction between "classical compact ellipticals" which have King/de Vaucouleurs profiles, and dEs and dIs which have more of an exponential profile. However, observations in the Virgo cluster show that most dEs are neither exactly exponential nor pure $r^{1/4}$ structures (Jerjen & Binggeli 1997).

The optical emission of the BCDGs is largely dominated by the young stars from the starburst, and this high brightness component masks the host galaxy structure in

Send offprint requests to: V. Doublier,
e-mail: vdoublie@eso.org

⋆ Based on observations made at 2.2 m Danish telescope in La Silla, operated by the European Southern Observatory.

Article published by EDP Sciences and available at http://www.aanda.org or http://dx.doi.org/10.1051/0004-6361:20000417

Table 1. Summary of the near infrared observations

Name	B mag.	Class.(*)	Observing date	total exposure (min) (J, H, K_s)	S/N at 22.5 mag arcsec^{-2}
Haro 14	13.92	d0	Dec. 95	18, 13, 6	2
Mk 996	15.35	e0	Dec. 95	20, 13, 27	2
Mk 600	15.47	e0	Dec. 95	47, 12, 34	2
Fairall 301	14.15	d0	Jan. 97	33, 25, 39	3
Tol 0610-387	16.02	cd	Dec. 95	27, 28, 80	2.5
Tol 0645-376	16.84	e0	Jan. 97	33, 25, 25	2.5
Tol 0954-293	15.76	cd	Jan. 97	25, 25, 30	2.5
Tol 0957-279	14.08	ce	Dec. 95	13, 10, 11	1.5
Tol 3	14.18	ce	Dec. 95	20, 10, 23	2
UM 465	14.37	d0	Jan. 97	33, 25, 30	3
UM 465 B	16.77	d0	Jan. 97	33, 25, 30	2.5
UM 461	16.18	cd	Jan. 97	32, 19, 25	2

(*): Photometric classification refers to Doublier et al. (1997).

the central region. Therefore, no quantitative information on the underlying stellar population can be obtained via imaging in the optical. The stars that will remain after the starburst fades, are intermediate and low mass stars from the present star formation event, and the evolved stars from previous bursts. They dominate the near infrared light, thus are best studied via photometric observation in J, H and K.

In this paper, we present the results of the surface photometry, in J, H and K_s[1], of 12 BCDGs. The galaxies were selected from our southern sample for which B and R surface photometry was presented in Paper II.

2. Observations and data reduction

Observations of 12 BCDGs were conducted at ESO-La Silla on the 2.2 m telescope, with the infrared camera IRAC2 a 256×256 pixel NICMOS chip. We used the focal configuration giving 0.507 arcsec/pixel with a field of view of 2×2 arcmin. Table 1 summarizes of the observations.

Column 1: Name of the object.
Column 2: Apparent B magnitude from Paper II.
Column 3: Photometric classification in the B band coded as follows: d0 have pure or almost pure exponential light profiles, cd have composite profiles with dominant exponential. e0 have pure or almost pure $r^{1/4}$ law profiles, ce have composite profiles with dominant $r^{1/4}$.
Column 4: Observing date.
Column 5: Total exposure time in minutes in J, H and K_s bands respectively.
Column 6: S/N, signal to noise ratio at isophotal level $K = 22.5$ mag arcsec^{-2}, in K_s band.
In the near infrared, we did not expect the observed size of our galaxies to exceed half the size of view the detector, therefore, we used the *in-field* chopping technique. The BCDG in our sample with the largest apparent diameter, has a radius of 60″ at $B = 27$ mag arcsec^{-2}. If only an evolved stellar population dominates at this radius, then $K \sim$ 23 mag arcsec^{-2} at $r \sim 60''$, which is below the detection limit of a ground-based 2 m class telescope. We obtained several mosaics for each galaxy in each band (JHK_s) with offsets of about 20″ in the East-West or North-South directions. The in-field chopping method is very effective because no time is lost for sky observations, thus allowing all of the time to be spent on the target. It also provides a better sky background subtraction because the sky background determination is made at the same position as the object and almost simultaneously. The observational strategy was to complete the observations for a given galaxy at least in a given filter per night, thus we did not have to combine images taken during different nights. Sequences of internal flat-fields in each band and bias exposures were obtained in the afternoon and in the morning, and dark exposures at the end of each night.

Each elementary frame was checked against all others within a given mosaic, and frames with large sky variations were rejected before combining the frames. The quality of the sky background varies from one mosaic to another because the weather conditions were not very stable. Moreover, for the combination of the frames, we used a strict rejection algorithm (minmax algorithm with high-rejection) to eliminate shadows of compact objects, like field stars, that remained on the sky background frames and would otherwise perturb the signal in the sky subtracted images. The sky subtraction procedure also accounts for bias subtraction and dark current removal. For flatfielding, we used the internal flatfields obtained before or after each observing night.

The biases were also used to produce a map of bad pixels, which is taken into account during the final combination of the frames. Since our strategy was to observe one band after the other, we could combine all frames at once, in each band for each galaxy.

Surface photometry was done using "user-built" procedures in MIDAS consistent with those used in the visible

[1] K_s is K short, it was wrongly named in the 2.2+IRAC2b manuals.

Fig. 1. K band contour plots and light profiles of the observed BCDGs. The outermost isophote corresponds to a signal-to-noise ratio of 1.75 (approx. 22 mag arcsec^{-2}), and spaced by 1 in units of S/N. The bar at the bottom of the contour plots represents 1 Kpc assuming $H_0 = 80$ km s^{-1}. The color profiles ($J-H$, $H-J$ and $J-K$) are displayed in individual graph for clarity. The bottom three graph show the J, H, K band light profiles as functions of the equivalent radius (in arcsec), the logarithm radius and the reduced $r^{1/4}$ radius. This figure is only available in electronic form at `http://www.edpsciences.org`

(see Paper I for a detailed explanation). Magnitude calibrations were performed using the standard stars from the Carter system observed at the same zenith distances as the galaxies. Since we observed the galaxies in the K_s band, we used the correspondence equations provided by the 2.2 m telescope Team (technical report IV: Lidman & Storm 1995) to transform the K_s magnitudes into the Carter K magnitudes.

3. Results of the photometry

Contour plots in K and the light distribution in each band, for each galaxy, are shown in Fig. 1. North is left and East is down. The outermost isophote corresponds to a signal-to-noise ratio of 1.75 (about 22 mag arcsec^{-2} for each BCDG) and the spacing of the contours is 1. in units of signal-to-noise ratio. The bar represents 1. kpc scale, at the assumed distance using $H_0 = 80$ Mpc km^{-1} s^{-1}. The other plots show the color distributions for $J-K$, $J-H$, and $H-K$, in individual graphs for clarity. The last 3 graphs show the light distributions for J (stars), H (squares) and K (diamonds), as functions of the equivalent radius (in arcsec), of the reduced scales $r^{1/4}$, and in logarithmic scale.

Table 2 shows the results of the surface photometry:

Column 1: Object Name.
Column 2: Asymptotic K magnitude, $J-K$ and $H-K$ asymptotic colors, derived by isophotal integration and curve of growth methods.
Column 3: Effective surface brightness in K, J and H, in mag arcsec^{-2}.
Column 4: Mean effective surface brightness in K, J and H within the half light radius $r_{\rm eff}$.
Column 5: Half light radius in arcsec in K, J and H.
Column 6: Radius at a quarter of the total luminosity in arcsec.
Column 7: Concentration index in K, J and H, defined as the ratio between $r_{0.25}$ and $r_{\rm eff}$ (de Vaucouleurs & Aguero 1973).
Column 8: Integrated magnitude in K, J and H within a 8″ aperture, for comparison with previous results (see below).
The magnitudes, and colors presented in this table, and on the plots of Fig. 1 are not corrected for galactic extinction.

3.1. Note on infra-red morphology

In Papers I and II, we found that the BCDGs could be classified into two groups depending on their light profiles: those dominated by an exponential law, and those dominated by an $r^{1/4}$ law. In the near-IR, two morphological types of BCDGs stood out: those with structures (e.g. Tololo 3, Fig. 1i) and those without (e.g. Mk 996, Fig. 1b). In the case of the former, most off-centered structures are associated with the star formation regions. Whether those structures would remain or not after the starburst has faded, is unclear. The presence of resolved sub-structures is mostly independent of the light profiles. The substructures seen in our BCDGs are generally smoother in the near-IR than in the optical bands (Papers I and II).

Some BCDGs which have regular envelopes in the optical do not have regular envelopes in the IR (e.g. Tololo 0610-387, Mk 600 Figs. 1e and 1c respectively). These irregularities could be due to the detection limit in the near-IR because the envelopes in the optical of these BCDGs are faint (below 24 mag arcsec^{-2} in the B band).

The main point is that BCDGs, in the near-IR, still do not look like dEs. The internal substructures are still visible, and obviously associated with the star forming regions. The case of Tololo 0610-387 reveals that these structures could in part be due to the presence of red supergiant stars, while in other BCDGs the infrared excess is most probably due to the contribution of the emission lines such as Brγ.

3.2. Color distributions

3.2.1. Integrated colors

The observed mean asymptotic color of our sample is *red*, $J-H = 0.74 \pm 0.47$, $J-K = 0.95 \pm 0.78$, $H-K = 0.21 \pm 0.85$ and $B-K = 3.03 \pm 0.89$. The large spreads are due primarily to Mk 600, UM 461 and Tol 0645-376. These galaxies show very peculiar structures similar to those of mergers and gravitationally interacting galaxies. They are very blue in the visible spectrum, clearly dominated by the starburst emission. For the other BCDGs, comparison with infrared colors of the different stellar types (Johnson 1966) indicates the presence of a dominating evolved stellar population, likely red giants of K and M types ($J-K \sim 0.64$, and $B-K \sim 3.40$ for a K0 red giant star). Figure 2a shows the color distribution of our sample.

Since the only available other photometric measurements for BCDGs have been done using an 8″ aperture (Thuan 1983; Hunter & Gallagher 1985), we simulated aperture photometry on the images of our BCDGs in order to compare our data with the results of those authors. We have carefully followed their procedure, i.e. searching for the brightest knot appearing on the visible image of the BCDGs and centering the aperture on it. The distribution of the colors in 8″ is shown in Fig. 2b, the arrows representing the mean values obtained by Thuan (1983) and

Table 2. Results of the near infrared surface photometry

Name	m_K	$\mu_{\rm eff}[K]$	$<\mu_{\rm eff}>[K]$	$r_{\rm eff}[K]$	$_{0.25}[K]$	$C_{21}[K]$	$m_K(8'')$
	$J-K$	$[J]$	$[J]$	$[J]$	$[J]$	$[J]$	$J-K(8'')$
	$H-K$	$[H]$	$[H]$	$[H]$	$[H]$	$H-K(8'')$	
Haro 14	10.80	21.68	18.53	14.0	6.3	2.23	13.05
	0.96	19.77	18.75	10.0	5.42	1.84	0.78
	0.47	19.12	18.15	9.4	4.9	1.95	0.18
Mk 996	11.64	20.03	18.64	10.0	3.6	2.81	13.13
	1.16	20.00	18.75	6.2	3.0	2.05	0.89
	0.74	19.55	18.32	6.2	2.6	2.37	0.42
Mk 600	14.39	19.50	18.93	3.2	1.84	1.75	15.19
	−1.04	21.16	20.22	9.6	4.8	2.0	0.0
	−1.23	21.05	19.97	9.2	5.0	1.84	0.02
Fairall 301	10.99	20.43	19.66	21.64	9.81	2.21	13.50
	1.25	20.71	19.98	16.35	6.42	2.55	0.85
	0.57	21.24	19.62	14.11	5.83	2.42	0.29
Tol 0610-387	12.36	22.32	19.78	12.2	5.9	2.05	14.48
	0.60	23.09	20.85	14.8	6.6	2.25	0.62
	−0.28	22.68	20.06	15.7	8.9	1.76	0.18
Tol 0645-376	13.45	20.31	19.62	6.87	3.66	1.88	14.62
	1.16	21.20	21.04	12.24	6.47	1.89	1.23
	−0.36	22.23	20.52	7.72	3.06	2.52	0.42
Tol0954-293	12.90	20.27	19.26	7.50	3.14	2.39	14.96
	0.77	20.57	20.52	9.59	3.80	2.52	0.98
	−0.25	21.89	19.55	9.41	3.55	2.65	−0.02
Tol 0957-279	10.56	20.05	18.95	19.0	10.7	1.77	13.55
	1.34	22.09	20.65	22.4	9.8	2.28	1.05
	1.15	20.28	19.64	15.4	6.6	2.32	0.03
Tol 3	10.78	18.38	17.39	8.3	4.2	1.99	12.25
	0.37	19.39	18.18	10.2	5.2	1.95	3.57
	−0.38	19.60	18.18	14.4	6.0	2.42	0.55
UM 465	10.37	18.30	17.42	10.29	7.74	1.33	12.06
	1.64	19.14	18.75	8.64	4.11	2.10	4.01
	1.19	19.60	18.23	9.93	4.51	1.98	1.03
UM 465B	12.43	18.71	17.83	4.81	3.37	2.03	13.56
	2.14	20.52	19.61	4.84	2.05	2.36	2.02
	1.52	20.58	19.37	4.07	2.05	1.98	1.41
UM 461	14.16	20.33	19.71	5.14	2.88	1.78	15.05
	0.99	21.07	21.31	10.49	6.06	1.73	1.26
	−0.68	22.16	20.58	6.82	3.49	1.95	0.56

Hunter & Gallagher (1985). The mean colors of our sample are even redder than theirs: $(J-K)_{8''} = 1.44 \pm 1.19$, $(J-H)_{8''} = 1.02 \pm 0.96$ and $(H-K)_{8''} = 0.42 \pm 0.43$. These high values are due to three of the BCDGs: Tol 3, UM 465A and UM 465B. Tol 3 presents two bright knots of star formation, the brightest in the visible being somewhat redder, it is centered with respect to the outer isophotes (both in the visible and in the infrared). This knot appears to be the nucleus of the host galaxy, and is composed of a significant fraction of evolved stars, both young red supergiants and old red giants (Terlevich et al. 1990). The same remarks apply to UM 465B because only the color indexes involving K band are affected. The red colors of UM 465A could be due to the presence of a dust lane visible across the central parts, as indicated by the high Balmer deficit observed: Hα/Hβ = 4.10 (Terlevich et al. 1991). When the three objects are removed from the statistics, our mean values compare statistically well with those of Hunter & Gallagher and Thuan.

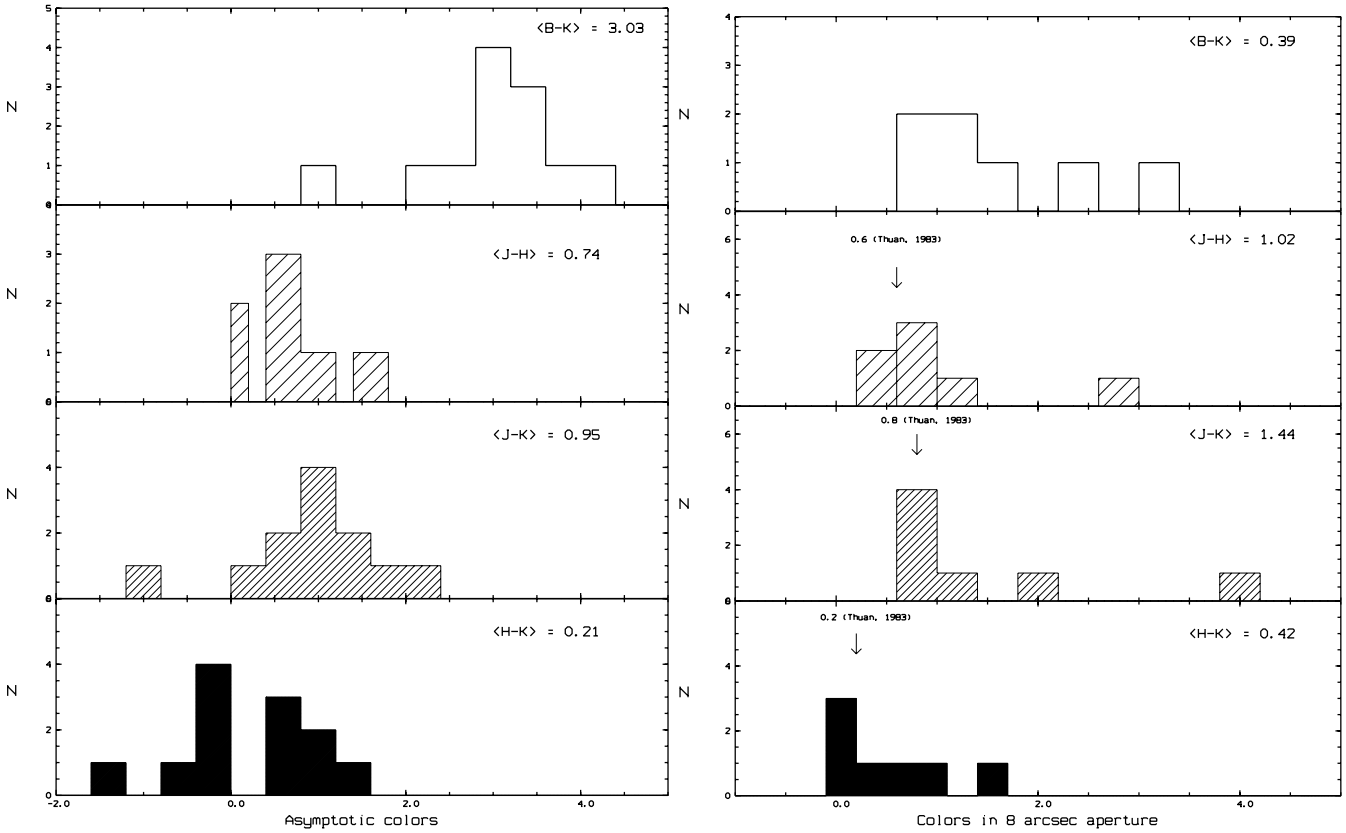

Fig. 2. **a)** Asymptotic-color distributions: open $B-K$, loose stripes $J-H$, dashed $J-K$ and filled $H-K$; **b)** integrated colors in an $8''$ aperture: open $B-K$, loose dashed $J-H$, tight dashed $J-K$, and filled $H-K$. The arrows represent the mean values obtained by Thuan (1983) and Hunter & Gallagher (1985)

We have studied the relations existing between the asymptotic color indexes. $J-K$, $B-K$ and $H-K$ are strongly correlated with each other, while $J-H$ appears to be constant for the $r^{1/4}$ BCDGs studied here, independent of the values of the other color indexes. Figures 3a and 3b show the different relations. On each diagram, we have indicated the location of a A0V star and of a K0III red giant.

The two photometric classes, $r^{1/4}$ (filled lozenge) and exponential (empty circle) BCDGs, show different relations. As seen in Figs. 3a and 3b, the excess in K is independent of the $J-H$ color index for the $r^{1/4}$ BCDGs. This is probably due to the fact that the $J-H$ index is very sensitive to metallicity and age. If $r^{1/4}$ BCDGs are the products of mergers and strong gravitational interactions, then we expect to observe very mixed populations of stars and metallicities, including intermediate age components. On the other hand, if exponential BCDGs are the products of slow accretion of gas without significant disturbance of the system, we expect to observe a gradient in the relative importance of the young starburst with respect to the evolved stars. This is characteristic of the degeneracy encountered for the predictions of integral colors in stellar population synthesis models (Charlot et al. 1996).

3.2.2. Asymptotic giant branch stars

While the mean colors of our sample are generally compatible with the presence of cosmologicaly ($\sim 10^{10}$ years) old stars, we note that, in many cases, the individual colors show a significant excess in the K band with respect to the optical bands. Figure 4a shows the optical-near-IR color-color diagram, the filled lozenges are the $r^{1/4}$ BCDGs, the open circles are the exponential BCDGs. The dashed line represent the zero age main sequence while the plain line represents the red giant branch stars, both for a solar metallicity. The BCDGs show a systematic excess in the K band of at least 1 mag with respect to the optical colors. This excess is seen with the effective colors. The star forming regions do not show this systematic excess (see next section). The optical images do not show any significant extended nebular emission either (Paper II). The K excess extends over the whole galaxy, the stars responsible for this emission should thus be distributed more or less smoothly throughout the galaxy: i.e. they have had time to diffuse in the gravitational potential. It takes between 10^8 to 10^9 years for a dense star cluster to diffuse within the galactic potential. The only stars that have a life time large enough to still be shining strongly in the near-IR after 10^8 years are the intermediate mass stars (i.e. with masses ranging between 2 $M_\odot$ and 10 $M_\odot$).

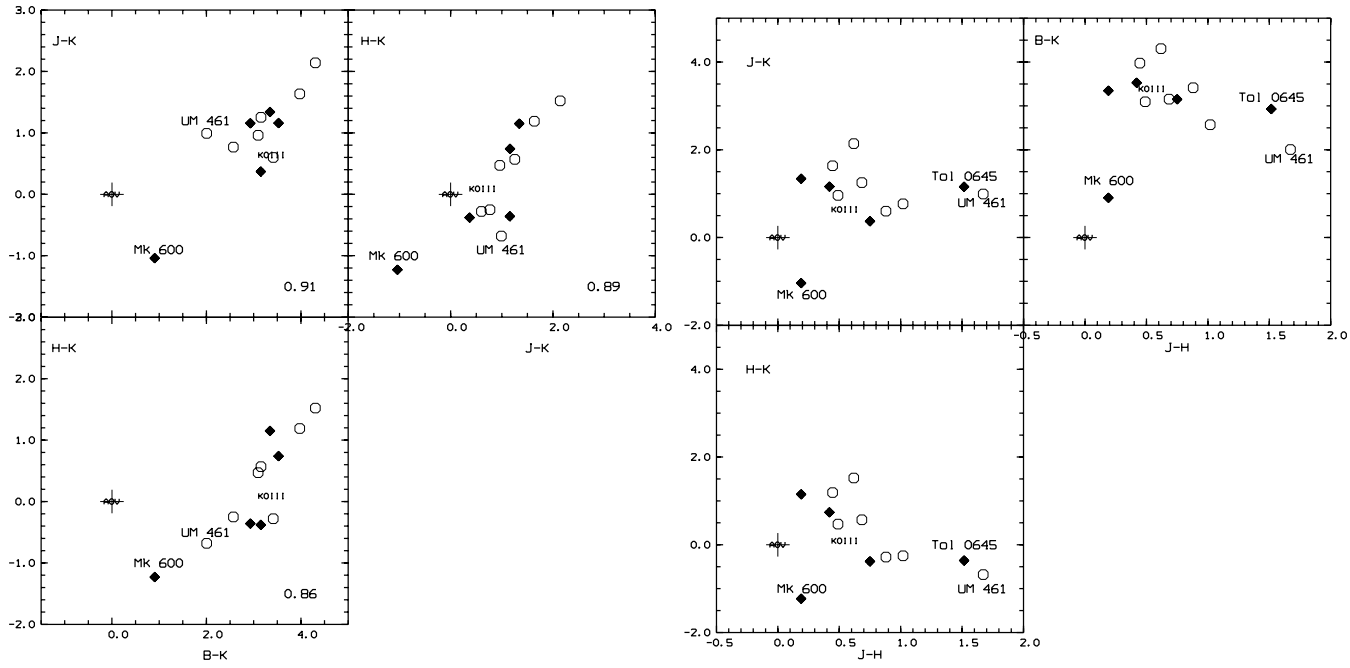

Fig. 3. a) Color-Color diagrams in the infrared: $B-K$ vs. $J-K$, $B-K$ vs. $H-K$ and $J-K$ vs. $H-K$. The locations of A0V and K0III spectral type star are plotted for comparison; **b)** color-color diagrams for $B-K$, $J-K$ and $H-K$ as functions of $J-H$ (sensitive to metallicity). The locations of A0V and K0III spectral type star are plotted for comparison

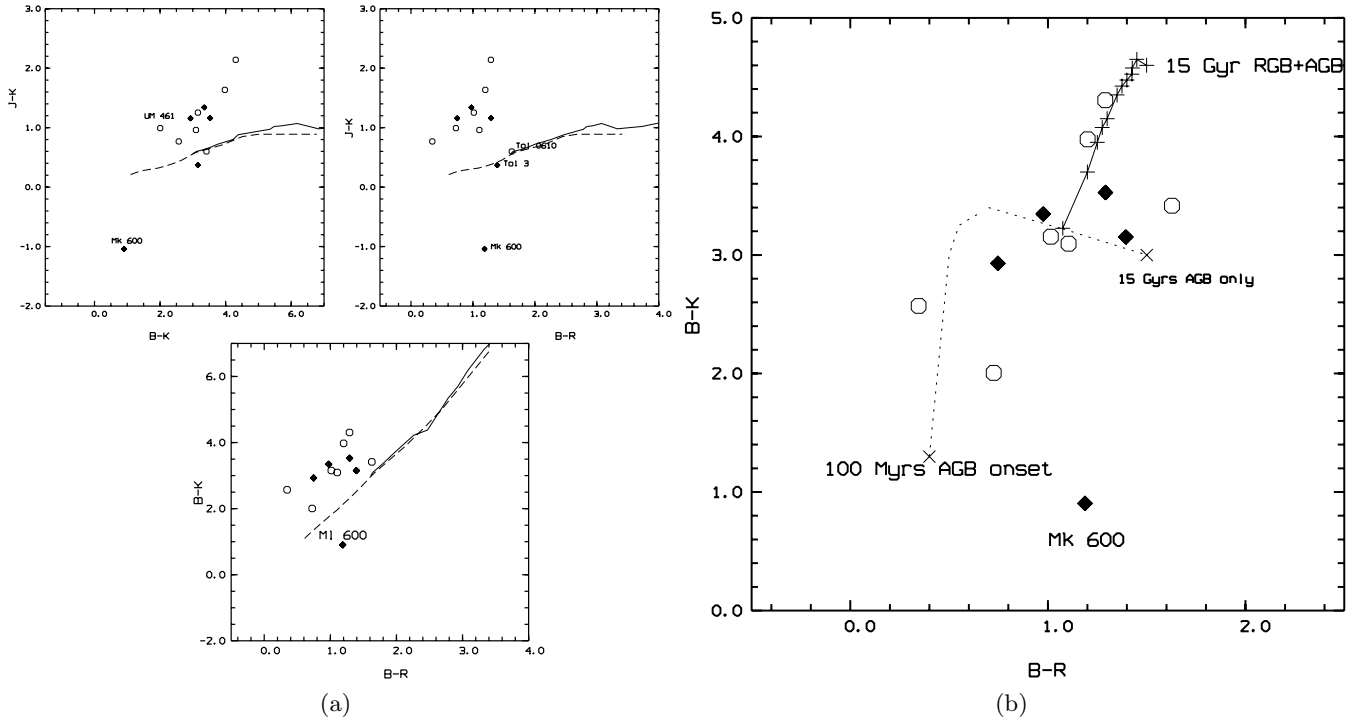

Fig. 4. a) Color-Color diagrams showing the excess in the K band. The open circles represent the exponential BCDGs, the filled lozenges represent the $r^{1/4}$ BCDGs. The lines plot the Color-Color diagrams of ZAMS (dashed) and red giant (continuous) stars for solar metallicity; **b)** $B-K$ versus $B-R$ color diagram. The open circles represent the exponential BCDGs, the filled lozenges represent the $r^{1/4}$ BCDGs. The dashed line represents the color evolution of a single stellar population including the onset of the AGB stars ($>10^8$ years). The continuous line represents the same stellar population including the onset of the RGB stars ($>10^9$ years). The data were taken from Bressan et al. (1998)

More specifically, asymptotic giant branch (AGB) stars. Following Girardi & Bertelli (1998), our excess in the IR color could be partly due to the AGB population, allowing us to set a lower limit to the age of our BCDGs of at least 10^8 years.

The question now is whether AGB stars alone, with ages ranging between 10^8 to 10^9 years, are enough to account for the total K emission. Again, following Girardi & Bertelli (1998), after 10^9 years, there is a second increase of the IR colors due to the onset of the red giant branch stars (RGBs). Figure 4b shows $B-K$ as function of $B-R$ color-color diagram. As for Fig. 4a the filled circles are the $r^{1/4}$ BCDGs and the open circles are the exponential BCDGs. The dashed line represents the color evolution of a single purely AGB population, the plain line represents the evolution of a single stellar population including the low mass stars below 2 $M_\odot$, both for low metallicity stellar populations. The tracks are derived from Bressan et al. (1998). The authors only give $B-V$ and $V-K$ colors as functions of time. To derive $B-R$ we applied a systematic $V-R$ of 0.3 typical for BCDGs (Telles & Terlevich 1997). After 10^9 years the red giant star population becomes dominant. Unless there is a continuous production of AGB stars which would require a significant underlying continuous star formation in some of our BCDGs, RGB stars have to be present in order to reproduce our excess in the near infrared. The presence of a diffuse population of AGBs is also consistent with the apparent lack of metallicity gradients of the gas in many BCDGs, and a very low continuous star formation (Legrand et al. 2000), as they would contribute to enrich homogeneously the interstellar medium over large scales.

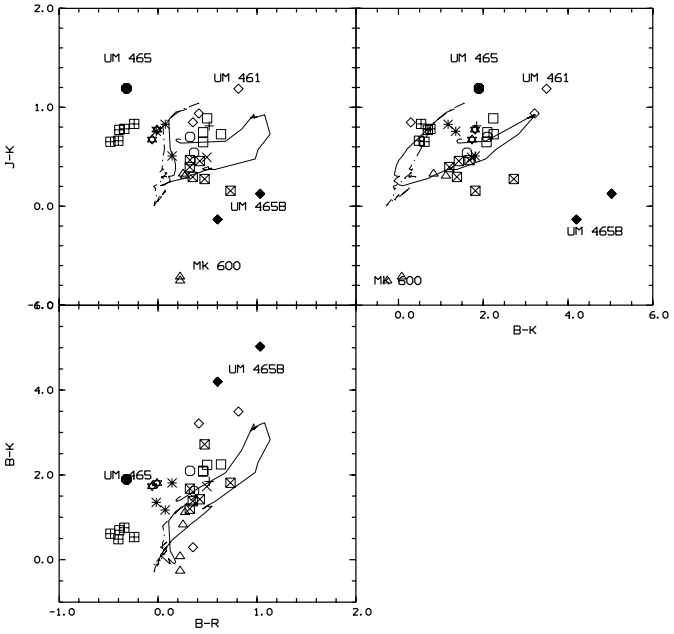

Fig. 5. Color-Color diagram for the star forming regions. Each symbol represent one galaxy: circle Fairall 301, square Haro 14, triangle Mk 600, cross (+) Mk 996, cross (×) Tol 0610-387, asterisk Tol 0645-376, star Tol 0954-293, crossed square (+) Tol 0957-279, crossed square (×) Tol 3, lozenge UM 461, filled hexagon UM 465A and filled lozenge UM 465B. The solid line represents the evolution of a starburst of solar metallicity, with a Salpeter IMF between 0 and 20 Myr from the population synthesis models of Cerviño & Mas-Hesse (1994). The dashed line represents the evolution of the same starburst with a lower metallicity of $Z = 0.08 z_\odot$

3.2.3. Star forming regions

We have studied the colors of the star forming regions in our 12 BCDGs. For each "blob", its spatial extent was determined from the $B-R$ map (Doublier et al. 1997, 1999). Variable-aperture photometry was performed on each blob, and the contribution of the underlying galaxy was systematically removed. We have corrected the colors both for Galactic extinction (Burstein & Heiles 1982) and from internal extinction derived from the spectroscopic data available in the literature (Terlevich et al. 1991; Izotov et al. 1994; Stasinska et al. 1996; Storchi et al. 1994). When the spectroscopic data were not available, we assumed a mean internal extinction for the HII regions of $E(V-B) = 0.2$ mag. The metallicity is assumed to be the same for all star forming regions inside a given galaxy, since mixing is probably very efficient across the small scale-lengths of the BCDGs (Marconi et al. 1994); also measurements in Tol 3 show that the ratio between oxygen and hydrogen is very similar from one star forming center to another (Stasinska & Leitherer 1996), even though they are some 300 pc apart.

Figure 5 shows the color-color diagrams for the star forming knots for the index $(J-K)$ versus $(B-R)$ and $(B-K)$, and for the index $(B-K)$ versus $(B-R)$. The solid line represents the variation of the color-color indexes as functions of time for a young starburst with a solar metallicity and a Salpeter Initial Mass Function (Cerviño & Mas-Hesse 1994). At lower metallicities (dashed line), the evolution is slightly shifted toward the lower-left corner since the metallicity affects the colors of the stellar populations such that at lower metallicity the stars appear bluer.

Each knot associated with a given BCDG is represented with the same symbol. For the majority of BCDGs, the different knots are clustered in small areas of the diagram. Taking into account the observational errors, this indicates that the star forming regions are probably of the same age (coeval) and thus derive from the same "starburst" event. However, for some BCDGs, the knots occupy different locations in the diagram. In the case of Mk 600, the differences in the location of the two knots indicate that the dominating populations in the knots differ in evolution.

Regions showing an excess both in R and K bands compared to the J band are most probably dominated by red giants. Since their positions in the BCDGs appear to be centered with the outer isophotes, they could be the nuclei of the galaxies (Tol 3, UM 465B and UM 461). An excess seen only in the K band probably indicates the

Table 3. Mean values of the photometric parameters in the near infrared

	N°	$< \mu_{\rm eff} >^*$ J mag/arcsec^2	$< \mu_{\rm eff} >$ H	$< \mu_{\rm eff} >$ K	$<r_{\rm e}>^*$ (K) kpc	$< I_{\rm e} >(K)$ $L_{\odot K}/{\rm pc}^2$	$< B-K >^*$
$r^{1/4}$	5	19.77 (1.24)	19.32 (0.91)	18.71 (0.82)	1002 (1185)	4406^{9376}_{2089}	2.8 (1.1)
Exponen.	7	19.97 (0.99)	19.37 (0.89)	18.89 (0.97)	688 (344)	3732^{9120}_{1527}	3.2 (0.7)

(*): Standard deviation of the sample is in parenthesis.

presence of young red supergiant stars, or dust-enshrouded star clusters.

A more complete analysis of the stellar populations in the star forming regions, and in the host galaxies will be given in a following paper.

3.3. Compactness index and mean surface brightness

The compactness index as defined by de Vaucouleurs & Aguero (1973) and Fraser (1977), $C_{21} = \frac{r_{0.5}}{r_{0.25}}$, varies little in our small sample: $< C_{21} > (K) = 2.02 \pm 0.37$, $< C_{21} > (J) = 2.16 \pm 0.26$ and $< C_{21} > (H) = 2.15 \pm 0.30$ (Fig. 6). The scatter in K is only due to the exponential BCDG UM 465 (face-on) with $C_{21}(K) = 1.33$ and the $r^{1/4}$ BCDG Mk 996 with $C_{21}(K) = 2.89$. Both galaxies represent almost the perfect photometric cases in K band (<1.9 for the spirals and >2.5 for the ellipticals, Fraser 1977). The otherwise small scatter in the values of $C_{21}(K)$ around $< C_{21} > \sim 2.0$ indicates that the starburst does not play a significant role in the stellar densities in our BCDGs. In the optical, we found that exponential BCDGs and $r^{1/4}$ had significantly different C_{21} values. Moreover, since the values for the concentration indexes are intermediate between "spirals" and "ellipticals" (Fraser 1977; de Vaucouleurs & Aguero 1973), it shows that BCDGs have more complex structures than previously believed.

The situation, however, is different in the J and H bands which are more sensitive to the young and intermediate age stars. $C_{21}(H)$ shows a spurious bimodal distribution possibly due to the small sample size. The $C_{21}(J)$ shows a flatter distribution.

Both bands are sensitive to the young main sequence stars of the starbursts, but also to the intermediate age population. In addition, the BCDGs for which $C_{21}(H)$ is larger than 2 have only one star forming region, while the BCDGs for which $C_{21}(H)$ smaller than 2 have at least 2 star forming regions. This could be simply a structural effect.

Similar remarks apply to the distribution of the mean surface brightness with the effective radius (Fig. 7: $< \mu_{\rm eff} >_K = 18.81 \pm 0.87$ mag arcsec^{-2} ($< I_{\rm eff} > = 4\ 10^3\ L_\odot/{\rm pc}^2$), $< \mu_{\rm eff} >_J = 19.88 \pm 1.05$ mag arcsec^{-2} and $< \mu_{\rm eff} >_H = 19.35 \pm 0.91$ mag arcsec^{-2}. Table 3 presents the mean values of our measured photometric parameters for the $r^{1/4}$ BCDGs and the exponential BCDGs, the photometric types being defined from the B band. Within the observed dispersion, the infrared values in both

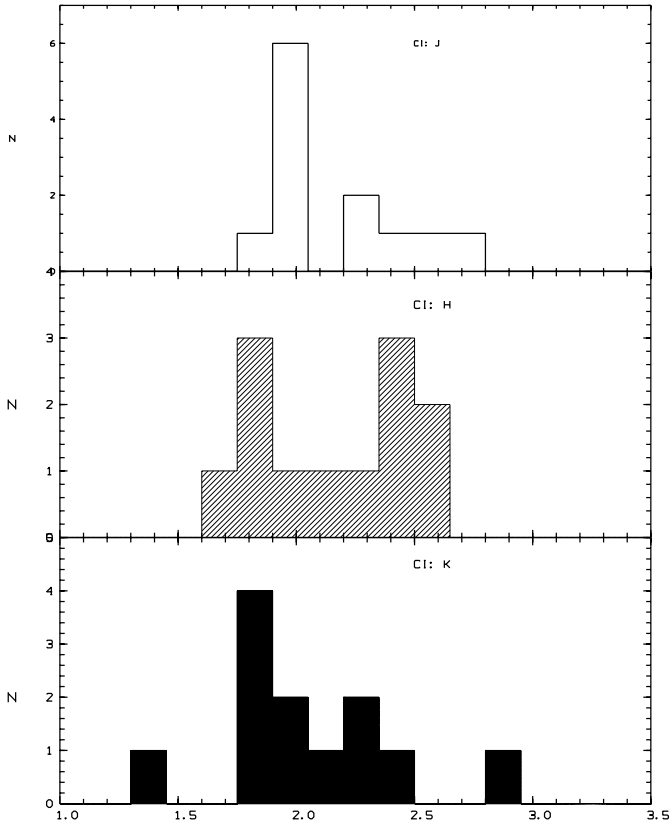

Fig. 6. Distribution of the compactness index C_{21} in each J, H and K band

photometric classes are very similar, while they were clearly different from class to class in the visible (Paper II). If the near infrared properties reflect what we can expect the BCDGs to look like after the burst has faded, then their mean photometric properties will not convey enough information to make out a clear dynamical classification. It follows that once the starburst has faded away, the remaining stellar distribution will not allow a strict photometric classification of the light profiles.

3.4. Brightness distributions

As seen from a comparison between Fig. 1 of this paper and Fig. 1 of Paper II, the light profiles in the infrared are generally consistent with the light distributions observed in the B and R bands. In some peculiar cases, however, the brightness profiles in J and K differ significantly from

Table 4. Absolute magnitudes and radii in the near infrared

Name	M_K	M_H	M_J	$R_{\rm eff}$[pc] (K)	$R_{\rm eff}$[pc] (J)	$R_{\rm eff}$[pc] (H)
Haro 14	−19.62	−19.15	−18.65	821	588	555
Mk 600	−16.12	−17.35	−17.16	197	586	562
Mk 996	−19.91	−19.17	−18.75	992	613	610
Tol 0610-387	−19.03	−19.29	−18.43	1113	1346	1432
Tol 0957-279	−18.04	−16.89	−16.70	483	571	391
Tol 3	−18.48	−18.86	−18.11	286	350	497
Fairall 301	−18.65	−18.08	−17.40	891	581	673
Tol 0954-293	−19.15	−19.40	−18.38	934	1171	1194
Tol 0645-376	−21.36	−21.72	−20.20	3049	3427	5430
UM 465A	−19.91	−18.72	−18.27	567	492	476
UM 465B	−17.85	−16.32	−15.71	265	225	267
UM 461	−15.60	−16.28	−14.61	223	296	455

the ones in the visible. Mk 996 shows a light distribution in J clearly dominated by an exponential law, while the profiles in H, K, B and R are dominated by an $r^{1/4}$ law. This galaxy thus presents two dynamically different components of different stellar population. The "exponential" component is clearly dominated by the starburst, while the $r^{1/4}$ component appears to be the old part of the galaxy. This behaviour strongly suggests a decoupling between the different dynamical components of the galaxies. The internal exponential component could have been created from slow gas infall, while the $r^{1/4}$ old component could originate from the formation of the galaxy itself, i.e. during isothermal gravitational collapse, or an equal mass merger.

In Fig. 1, considering all objects with respect to what is seen at visible wavelengths, the structures are less pronounced, the central peak is less significant in the near infrared than in the visible. The color profiles show a striking property though: the $J-K$ (open circles) and $J-H$ profiles (filled lozenge) of the $r^{1/4}$ BCDGs decrease then increase with increasing radius, while the $H-K$ profiles (open square) remain monotonic (e.g., Mk 996). The $J-K$ and $H-K$ profiles of the exponential BCDGs decrease monotonically while $J-H$ decreases then increases with increasing radius (e.g. Haro 14). This implies that the distribution of the stellar populations varies from one photometric type to the other, i.e. the young stars being more concentrated in the center of the $r^{1/4}$ BCDGs than in the exponential BCDGs.

The colors of the central regions do not vary much from one BCDG to another ($(J-K)_{\rm c} \sim 1.0$, $(J-H)_{\rm c} \sim 0.5$, and $(H-K)_{\rm c} \sim 0.$), except for Mk 996, which has a dust lane obscuring partly the nucleus (Thuan et al. 1996), and Mk 600 which is very blue. The $B-K$ color profiles reach a limiting value at the outermost K isophote, similar for all our BCDGs: $B-K \sim 4.6$, while the central value is similar for the all the BCDGs: $B-K \sim 2.6 \pm 0.1$ (NOT corrected for Galactic extinction). Correcting the observed values for Galactic extinction, the $< B-K > \sim 1.7$ mag corresponds to the values measured for the star forming regions (see Fig. 7).

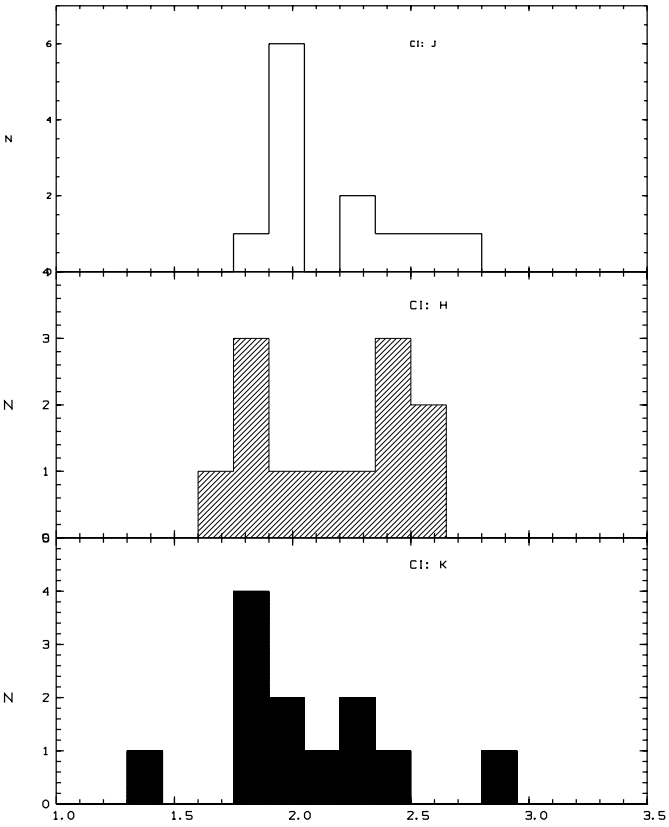

Fig. 7. Distribution of the mean effective surface brightness in each J, H and K band

4. Radius – absolute magnitude relation

Table 4 summarizes the absolute magnitudes and linear radii for the BCDGs in the near infrared. The values were computed using $H_0 = 80$ Mpc km^{-1} s^{-1}. No k-correction was applied since at such low recession velocities, it is largely negligible.

We saw in the previous section that the light distribution in the near infrared is less sensitive to the starburst than in the optical, especially in K band. We have investigated the relation between the absolute magnitude and the radius in the three bands. Figure 8a shows the relations for the radius at 50% ($r_{\rm eff}$) of the total infrared

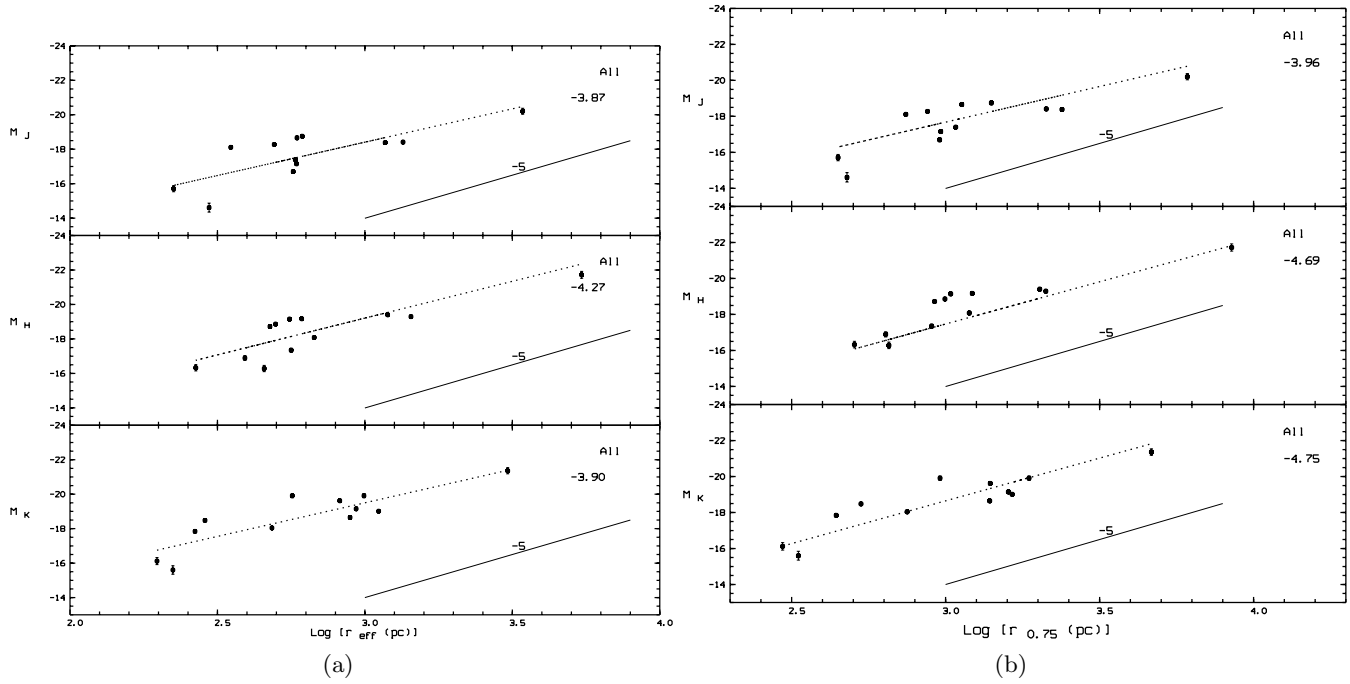

(a) (b)

Fig. 8. a) Magnitude – radius relation at the effective radius $r_{\rm eff}$, in pc in each band J, H and K. The continuous line represents the empirical -5 relation, the dotted line represents the least square fit to the data. The slope of the fit is indicated in the upper right corner; **b)** magnitude – radius relation at $r_{0.75}$ in pc, in each band J, H and K. The continuous line represents the empirical -5 relation, the dotted line represents the least square fit to the data. The slope of the fit is indicated in the upper right corner

Table 5. Relation between absolute magnitude and radius in the bands J, H and K

	A	σ
	$r_{0.5}$	
J	$-4.88(0.46)$	$-3.87(0.13)$
H	$-4.60(0.37)$	$-4.27(0.09)$
K	$-4.64(0.33)$	$-3.90(0.31)$
	$r_{0.75}$	
J	$-4.86(0.38)$	$-3.96(0.11)$
H	$-4.82(0.28)$	$-4.69(0.12)$
K	$-4.58(0.29)$	$-4.75(0.13)$

A: slope of the relation.
σ: slope of the relation after 1 sigma rejection.

light and Fig. 8b shows the relations for the radius at 75% ($r_{0.75}$) of the total infrared light. Table 5 summarizes the coefficients of the relations and the correlation coefficients in the three bands for both radii.

The coefficients of the $r_{\rm eff}$ relation are significantly smaller than the -5.0 empirical value after 1 sigma rejection, possibly due to a systematic effect as in the B band (Papers I and II) but the size of the sample is small and the statistical significance is low. Moreover the slope of the relation depends strongly on the quality of the determination of the effective radius based on the extrapolation to estimate the asymptotic magnitudes, although this would mainly affect the scatter of the points. It depends also on the intrinsic morphology of the objects, e.g. the compactness. For example, in the cases of Tol 0957-297 and Fairall 301. Both have about the same physical size ($R_{26} \sim 2$ kpc), but they have very different compactness indexes in B and R bands: Tol 0957-279 shows a very steep decreasing luminosity gradient in the R band, about twice the gradient observed in Fairall 301. If the stellar densities drop so much in Tol 0957-297 compared to Fairall 301, we do not expect to be able to detect the emission very far out from the starburst in K (we detect the K emission to $30''$ compared to the $50''$ radius of the galaxy in B). Hence, the determination of the radii will be strongly affected by the presence of the burst. The starburst affects the relation such that the smaller galaxies show a central excess in the near infrared compared to the larger galaxies.

In the case of $r_{0.75}$, the values in all three bands are significantly closer to the empirical value, supporting the idea that the near infrared bands are much less affected by the starburst than in the optical. At large radii, the evolved host galaxy dominates in all bands, confirming the previous results obtained in the R bands (Papers I and II).

We are interested in understanding the relations between the photometric class and the intrinsic parameters. Table 6 summarizes the absolute magnitude-radius relation in all 5 bands (B, R, J, H and K) for both classes of BCDGs.

The slope of the relation is very different between the two classes. The smaller $r^{1/4}$ BCDGs show a significant excess of light dominated by the starburst, especially in the B and R bands, but not in K band. On the other hand,

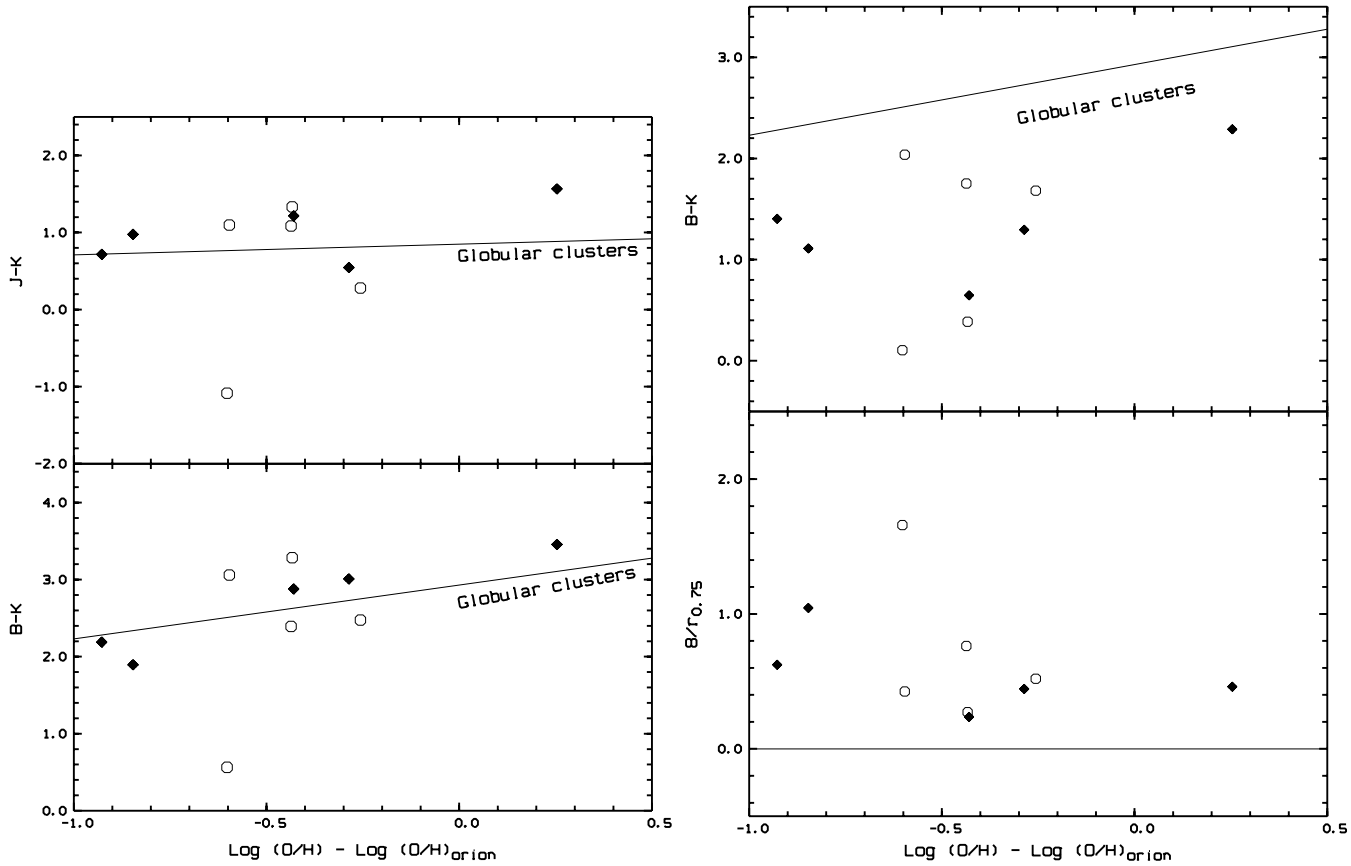

(a) (b)

Fig. 9. a) Color-Metallicity relation for the BCDGs compared to the relation described by the globular clusters (continuous line). The $r^{1/4}$ BCDGs are represented in filled lozenge, the exponential BCDGs are represented in open circles; **b)** upper panel: color – metallicity relation in an $8''$ aperture. The continuous line represents the relation followed by the Globular Clusters. Lower panel: effect of the integration in an aperture on the color metallicity relation. We plotted the ratio between the $8''$ aperture and the size of the BCDGs at 75% of light as a function of the metallicity. The $r^{1/4}$ BCDGs are represented in filled lozenge and the exponential BCDGs are represented in open circles

the exponential BCDGs follow loosely the empirical relation as indicated by the low correlation coefficients. The scatter in the relation may be due to the fact that in our exponential BCDGs, the star formation is spread throughout the galaxy, while in $r^{1/4}$ BCDGs the star formation takes place mostly in the central regions.

The scatter, in the relations, is smaller for the $r^{1/4}$ BCDGs. Again, it is probable that the steepness of the slope is due to the fact that the starburst dominates the smaller BCDGs, and the small scatter may be due to the fact that the star formation appears to take place in localized and compact regions.

Table 6. Relation between the absolute magnitude and $r_{0.75}$ for the two photometric classes

	$r^{1/4}$		Exponentials	
$r_{0.75}$	A	ρ	A	ρ
B	−3.71(0.10)	0.98	−6.48(0.71)	0.38
R	−3.52(0.17)	0.94	−5.83(0.61)	0.44
J	−3.78(0.86)	0.76	−5.71(0.61)	0.79
H	−4.10(0.52)	0.90	−5.56(0.65)	0.77
K	−4.20(0.40)	0.94	−5.39(0.64)	0.77

A: slope of the relation after 1 sigma rejection.
ρ: correlation coefficient.

5. Metallicity – color relation

Our 12 BCDGs follow tightly the "color-metallicity" relation described by the Galactic globular clusters (Aaronson et al. 1978) as shown in Fig. 9a, where the colors $J-K$ and $B-K$ versus the metallicity index $[\mathrm{O/H}] = \log(\mathrm{O/H})/\log(\mathrm{O/H})_{\mathrm{orion}}$ are plotted. The [O/H] abundances are derived from the spectroscopic data taken from Terlevich et al. (1991); Pagel et al. (1992); Izotov et al. (1994); Masegosa et al. (1994); Sortchi-Bergmann et al. (1995) and Stasinska et al. (1996). This contrasts with the results obtained by Thuan (1983) and Hunter & Gallagher (1985), who both find that their BCDGs and HII galaxies

are "younger" than the globular clusters. But as shown in Fig. 9b, if we plot the same relation for a simulated 8″ aperture photometer centered on the brightest knot, we also find that the colors are "bluer" than the globular clusters, which is expected since the aperture of 8″ accounts only for the starburst. The lower panel of the figure shows how the ratio between the aperture size equal to 8″ and the radius $r_{0.75}$ at 3/4th of the total light of the BCDGs. In the near infrared, it varies with the metal content in our BCDGs. The observed 8″ aperture relation, is thus somewhat spurious, and only shows the relative importance of the starburst emission within that aperture.

The large scatter in our data indicates the presence of an intermediate age stellar population, possibly AGB stars (as discussed above), whose contribution depends on the star formation history of the BCDGs. For comparison, our BCDGs' behaviour resembles of the LMC globular clusters whose ages vary from 10^8 to 10^{10} years for the same range of colors.

Again, the question of the degeneracy between age and metallicity cannot be fully resolved. For instance, recent results obtained by Gallagher et al. (1998) for the moderately star forming dwarf Pegasus show a large population of red giant stars bluer than their metallicity would suggest. Hence, the authors suggest that the bulk of the RGB stars were formed about 2 Gyrs ago. If we dismiss the Color-Metallicity diagram, the blue IR colors of some BCDGs indicate that the bulk of the underlying galaxy was formed only a few Gyrs ago, and is responsible for the observed metallicity. If we assume that the observed metals originate from an earlier burst then the present day metals are hidden in the hot phase (Tenorio-Tagle 1996).

However, in Sect. 3.3.2, we showed that the excess of IR was due to a non-negligible population of Red Giants stars of at least 5 Gyrs for a solar metallicity, hence much older at our lower metallicities. Studies are under way to determine the metallicities of the different stellar components and compare them with the gas metal content.

6. Conclusion

Eleven out of twelve BCDGs in our sample are dominated by an old stellar population. This rules out the "genuine young system" hypothesis for those BCDGs (in the sense of "primeval" character). In the case of Mk 600, the emission is dominated by the starburst even in the near-infrared. Nonetheless, Mk 600 follows the same color-color relations as the other BCDGs, hence an evolved stellar population must be present, although its emission is hidden by the starburst.

The BCDGs follow the same color-metallicity relation as the Galactic globular clusters, indicating that the underlying stellar population of these BCDGs is dominated by a stellar population similar to those of the globular clusters given the metallicity of the stars.

We found that BCDGs host significant AGB populations in addition to a cosmologicaly old red giant star population. The origin of the AGBs remains uncertain, i.e. whether they come from older busts, or from a very low continuous star formation.

The photometric classification described in Papers I & II still holds in the near infrared, but the dichotomy between the two classes as measured by the infrared photometric parameters is less obvious. Also, we found that some peculiar cases, like MK 996 showing an almost pure exponential in the J band, and UM 465 showing a significant $r^{1/4}$ law envelope in all three bands. We find that the $r^{1/4}$ BCDGs follow a tight relation between the absolute magnitude and the radius, but the small BCDGs show a systematic excess of light for their effective size compared to the larger BCDGs. On the contrary, the exponential BCDGs show a loose relation between the absolute magnitude and the radius, but they don't show any size dependent color "excess".

References

Aaronson, M., Cohen, J. G., Mould, J., & Malkan, M. 1978, ApJ, 223, 824
Bressan, A., Granato, G. L., & Silva, L. 1998, A&A, 332, 135
Burstein, D., & Heiles, C. 1982, AJ, 87, 1165
Cerviño, M., & Mas-Hesse, J. M. 1994, A&A, 284, 749
Charlot, S., Worthey, G., & Bressan, A. 1996, ApJ, 457, 625
de Vaucouleurs, G., & Aguero, E. L. 1973, PASP, 85, 150
Doublier, V., Caulet, A., & Comte, G. 1999, A&AS, 138, 213
Doublier, V., Comte, G., Petrosian, A., Surace, C., & Turatto, M. 1997, A&AS, 124, 405
Ferguson, H. C., & Binggeli, B. 1994, A&AR, 6, 67
Fraser, C. W. 1977, A&AS, 29, 161
Gallagher, J. S., Tolstoy, E., Dohm-Palmer, R. C., et al. 1998, AJ, 115, 1869
Girardi, L., & Bertelli, G. 1998, MNRAS, 300, 533
Hunter, D. A., & Gallagher, J. S., I. 1985, AJ, 90, 1457
Izotov, Y. I., Thuan, T. X., & Lipovetsky, V. A. 1994, ApJ, 435, 647
Jerjen, H., & Binggeli, B. 1997, in The nature of Elliptical Galaxies Proc. of the second Stromlo symposium, ed. M. Arnoboldi, G. S. DaCosta, & P. Saha
Johnson, H. L. 1966, ARA&A, 4, 193
Kunth, D., & Sargent, W. L. W. 1986, ApJ, 300, 496
Legrand, F., Kunth, D., Roy, J., Mas-Hesse, J. M., & Walsh, J. R. 2000, A&A, 355, 891
Lidman, C., & Storm, J. 1995, ESO Observing Reports
Marconi, G., Matteucci, F., & Tosi, M. 1994, MNRAS, 270, 35
Masegosa, J., Moles, M., & Campos-Aguilar, A. 1994, ApJ, 420, 576
Pagel, B. E. J., Simonson, E. A., Terlevich, R. J., & Edmunds, M. G. 1992, MNRAS, 255, 325
Papaderos, P., Loose, H. H., Fricke, K. J., & Thuan, T. X. 1996, A&A, 314, 59
Stasinska, G., & Leitherer, C. 1996, ApJS, 107, 661
Storchi-Bergmann, T., Calzetti, D., & Kinney, A. L. 1994, ApJ, 429, 572
Storchi-Bergmann, T., Kinney, A. L., & Challis, P. 1995, ApJS, 98, 103

Telles, E. 1996, PASP, 108, 462
Telles, E., & Terlevich, R. 1997, MNRAS, 286, 183
Tenorio-Tagle, G. 1996, AJ, 111, 1641
Terlevich, E., Diaz, A. I., Pastoriza, M., Terlevich, R., & Dottori, H. 1990, Rev. Mex. Astron. Astrofis., 21, 192
Terlevich, R., Melnick, J., Masegosa, J., Moles, M., & Copetti, M. V. F. 1991, A&AS, 91, 285
Thuan, T. X. 1983, ApJ, 268, 667
Thuan, T. X., Izotov, Y. I., & Lipovetsky, V. A. 1996, ApJ, 463, 120
Thuan, T. X., Izotov, Y. I., & Lipovetsky, V. A. 1997, ApJ, 477, 661
Thuan, T. X., Sauvage, M., & Madden, S. 1999, ApJ, 516, 783